Colloid Polym Sci (2008) 286:3–14
DOI 10.1007/s00396-007-1728-3

ORIGINAL CONTRIBUTION

Metal nanoparticle formation on layer silicate lamellae

Szilvia Papp · Rita Patakfalvi · Imre Dékány

Received: 9 February 2007 / Revised: 16 June 2007 / Accepted: 18 June 2007 / Published online: 14 August 2007

Abstract Nanoparticles (Ag, Pd) were prepared by heterogeneous nucleation on the interlayer space of layered montmorillonite and kaolinite minerals in aquatic dispersion. Interlamellar incorporation of nanoparticles was monitored by X-ray diffraction and verified by transmission electron microscopy (TEM). After the reduction of adsorbed metal ions, a new Bragg reflection appeared, proving the formation of nanoparticles in the interlamellar space of clay mineral. Lamellar structure of layered silicates is partly destroyed by the particle formation. TEM images showed that larger nanoparticles were formed by UV irradiation and hydrazine hydrate than in the case of reduction by $NaBH_4$. Aqueous solutions of polyvinyl pyrrolidone and clay minerals were used for the stabilization of Pd° nanoparticles. The size of particles generated on the surface of clay minerals by heterogeneous nucleation increased with increasing metal concentration. When polymer is added to this system, particle size can be decreased by increasing polymer concentration. In this case, the particles are stabilized by the concerted action of the support and the macromolecule. The polymers promoted intercalation of nanoparticles into the clay mineral. In the absence of nanoparticles, the intercalation of polymers was significantly less extensive.

Keywords Palladium · Silver · Layered silicate · Nanoparticle formation · XRD · TEM

S. Papp · R. Patakfalvi · I. Dékány
Supramolecular and Nanostructured Materials Research Group of the Hngarian Academy of Sciences, Szeged, Hungary

I. Dékány (✉)
Department of Colloid Chemistry, University of Szeged, Aradi Vértanúk tere 1, 6720 Szeged, Hungary
e-mail: i.dekany@chem.u-szeged.hu

I. Dékány
Bay Zoltán Foundation for Applied Research, Institute for Nanotechnology, 3519 Miskolc, Iglói út 2, Hungary

Introduction

The preparation and characterization of precious metal nanoparticles have moved into the focus of cutting-edge research in the last few decades. Scientists have recognized that the physical and mechanical properties of nanosize particles differ from those of macroscopic material. Precious metal nanoparticles are mainly utilized in solving the problems of catalysis and hydrogen storage.

John Bradley [1] classified reactions that have so far been utilized for the preparation of transition metal particles into four groups corresponding to four types of methods. Due to its simplicity and effectivity, the currently most preferred preparation method is liquid-phase reduction of metal salts. The reducing agent employed is mainly hydrogen gas [2, 3], hydrazine [4, 5], or sodium borohydride [6, 7], but citrate [8, 9], hypophosphorous acid [10], and oxidizable solvents such as alcohols [11, 12] have also been successfully used in synthetic reactions. It is essential that aggregation be prevented in the course of preparation; in this way, the synthesis of even very small particles (in the size range of a few nanometers) becomes possible. The most widely used techniques make use of the physical limitations of the preparation environment, like in reactions staged inside inverse micelles [13, 14], porous solid materials [15], gels [16], polymers [17], or dendrimers [18].

There is nowadays an ever-increasing need for metal catalysts on solid supports. Many different physical methods (pulse laser evaporation, electron beam lithography) and chemical procedures are available for the preparation of supported catalysts. These are mainly prepared by the impregnation technique, preferred due to its simplicity. In the course of the procedure, the metallic precursor is first impregnated on the support and later reduced. The impregnation technique, however, does not allow control of the size, morphology, and surface distribution of nanoparticles. Methods generating nanoparticles by colloid chemical means are becoming more and more widespread. One of the most practical of these is the preparation of metal sols and their deposition on supports. At the first stage of the procedure, a stabilized dispersion of metal particles is produced by reduction; the particles are next bound to a support, and finally the product is washed. The main advantage of this method is that particle size is independent of the support. Bönnemann et al. [19] adsorbed transition metal particles synthesized in tetrahydrofurane, stabilized by quaternary ammonium salts, on the surface of charcoal. Reetz applied electrochemically obtained colloids on charcoal, silica, and alumina supports using two different methods [20, 21]. He added the support to the reaction medium either in the course of particle formation or after the completion of the electrochemical reaction. He established by transmission electron microscopy (TEM) of the support-bound particles that neither their structure nor their size was altered during adsorption in either case. Wang et al. [22, 23] bound polyvinyl pyrrolidone (PVP)- and poly (vinyl alcohol)-stabilized Pd, Pt, and Rh particles to silica surfaces. They interpret binding as joint adsorption of the polymer and the metal particles. Polymer adsorption is due to hydrogen bonding with the hydroxyl groups of silica.

Another possibility for the preparation of nanosize particles is in situ synthesis within the solid–liquid interface of sols and dispersions, using the adsorption layer on the surface of solid particles as "nanoreactors". Layer silicate minerals with large internal surfaces, readily swelling in aqueous media, lend themselves well to the preparation of particles with diameters of a few nanometers not only on their surfaces, but—under suitable conditions—also within their interlamellar space [24–26].

The so-called solid/liquid interface nanoreactor technique enables in situ formation and stabilization of metal foci on the surface of the support. Király et al. [26] synthesized Pd particles (2–14 nm) in situ in organophilized montmorillonite (HDAM) in an ethanol–toluene binary mixture. After the establishment of the adsorption equilibrium, they added $Pd(OAc)_2$ solution in 1% toluene to the dispersion. At the appropriate ethanol/toluene ratio, ethanol is preferentially adsorbed in the interlamellar space (acting as a nanophase reactor) and reduces Pd^{2+}ions transported there by diffusion. A similar procedure was used for the preparation of Pd subcolloids measuring 4–10 nm in diameter on pillared clay minerals [27]. In addition to in situ synthesis, this method is also successfully applicable to the adsorption of fully-grown particles on supports [28].

In the course of this work, we synthesized silver and palladium particles using methods successfully applied earlier as well as others developed in our laboratory; we studied the possibilities of control over particle size offered by the various methods. We prepared nanoparticle/support composites by heterogeneous nucleation on the surface and in situ in the interlamellar space of montmorillonite and kaolinite. We use the stabilizing effect of the polymer/clay mineral complex in the course of nanoparticle formation. The effect of the incorporation of nanoparticles into ordered lamellar structures was studied by X-ray diffraction (XRD). Particle size was determined by TEM and surface oxidation state by X-ray photoelectron spectroscopy (XPS). In parallel with in situ nanoparticle synthesis on the surface of montmorillonite, adsorption of the polymer stabilizers on Na–montmorillonite was also studied.

Materials and methods

Materials

Precursors: $AgNO_3$ (Reanal, 99.9%), $PdCl_2$ (Aldrich, 99%)
Reducing agents: ethanol (C_2H_5OH, p.a., Reanal), hydrazine hydrate ($NH_2NH_2{\cdot}H_2O$, 24–26% (*m*/*m*) aqueous solution, Fluka), sodium borohydride ($NaBH_4$, 99%, Aldrich)
Stabilizing agents: PVP (M_w=40,000, Fluka)
Supports: Na–montmorillonite (Süd-Chemie AG, Germany, $a_{BET}^{S} = 87.7\ m^2/g$) and kaolinite (Zettlitz, Germany, $a_{BET}^{S} = 14\ m^2/g$)
Other compounds used: dimethyl sulfoxide (DMSO, a.r., Reanal), methanol (CH_3OH, a.r., Reanal)

Methods

Ultraviolet-visible absorption spectroscopy Ultraviolet-visible (UV-VIS) absorption studies were performed in an Uvikon 930 dual-beam spectrophotometer. Measurements were made in 1-cm quartz cuvettes in the wavelength range of 200–800 nm. Adsorption of nanoparticles on clay minerals was followed by measuring the spectrum of the supernatant.

X-ray diffraction Basal spacing of the nanoparticle/clay mineral intercalation structures and the size of metal

crystallites were determined by large-angle XRD in a Philips X-ray diffractometer (PW 1830 generator, PW 1820 goniometer, CuK-α radiation: λ=0.1542 nm, 40 kV, 25 mA). The values of basal spacing (d_L) were calculated from the first-order reflections (001) by the Bragg equation ($d_L=\lambda/2\sin\Theta$) with the help of the APD 3.5 automatic X-ray diffraction software. The average diameter of metal crystallites was calculated from the line broadening of the (111) reflection using the Scherrer equation: $d=k\lambda/\beta\cos\Theta$, where k is the constant characteristic of particle shape (k=0.9), λ is the wavelength of X-ray radiation, and Θ is the angle of reflection. β equals the difference of the line breadth determined for the given sample (β_S) and that determined for the macrocrystalline material (β_0). This calculation was also performed by the Philips PC-APD 3.5 program.

Transmission electron microscopy Size analysis of Ag nanoparticles was carried out in a Philips CM-10 electron microscope (acceleration voltage 100 kV) equipped with a Megaview-II digital camera. Solid samples were studied in dilute aqueous dispersions, whereas in the case of sols, droplets of the undiluted material were placed on Formwar-coated copper mesh grids (diameter 2 mm). The average particle diameter and size distribution of the samples were determined by the UTHSCSA Image Tool 2.00 software, based on the data of an average of 200 particles. The maximal resolution of the microscope is approximately 0.2 nm.

X-ray photoelectron spectroscopy Measurements were performed in the ultrahigh vacuum chamber ($p = 2 \times 10^{-9}$mbar) of a Kratos XSAM 800 instrument equipped with a hemispherical analyzer. Al K_α radiation ($h\nu$=1,486.6 eV) was used as the excitation source. The gun was operated at 15 kV, 15 mA. The pass energy of the electron analyzer was set to 40 eV, and the step width between the channels was 50 meV. Usually ten scans were added to give a single spectrum. All binding energies were referenced to the C (1s) line of the adventitious carbon assumed to have a constant binding energy of 285.1 eV. Data acquisition and evaluation were performed with the VISION 1.3.3 software provided by Kratos.

We determined the adsorption isotherm of PVP, necessary for stabilization of sols, on montmorillonite. Na–montmorillonite was dispersed in polymer solutions of various concentrations, and the dispersions were stirred at room temperature for 2 days until adsorption equilibrium was reached. The suspensions were centrifuged, and the carbon content of the polymer solution (supernatant) was determined by total carbon (TC) measuring system. Equilibrium concentrations of polymers were determined by calibration measurements. The amount of bound polymer was calculated as the difference of the initial (c_0) and post-adsorption (c_e) concentrations. Montmorillonite concentration in the suspensions was 1 g/100 cm^3 in all cases. The amount of adsorbed polymer was calculated by the relationship $n^s_{pol} = V^\circ(c_0 - c_e)$ / m, where V° is the volume of the polymer solution and m is the mass of montmorillonite. Amounts of adsorbed material were determined in the concentration range of 0.025–2.5 g/100 cm^3.

Total carbon measurements The amount of polymer adsorbed on the clay minerals was determined indirectly, based on the total carbon content of the supernatants of the samples after adsorption. The measurements were performed in a Euroglas 1200 apparatus. The determination is based on infrared detection of carbon dioxide generated by incineration of the sample at 1,000°C in high-purity oxygen–argon atmosphere. The apparatus can be used for direct determination of carbon content in solutions and dispersions in the range of 0.5–1,000 ppm.

Photochemical reaction Photoreduction of Ag^+ ions was carried out with an Osram xenon lamp (P=75 W). The dispersions were irradiated from an identical distance for identical times (1 h). In the course of photoreduction, Ag^+ concentration was set to bring the amount of silver added to 1, 2, 5, and 10 g/100 g kaolinite. The suspension was placed in a quartz beaker and irradiated with a xenon lamp (P=150 W) from a distance of 10 cm for 1 h under constant stirring.

Results and discussion

Particle size control on clay minerals

Synthesis of palladium nanoparticles on montmorillonite

For the preparation of Pd-containing montmorillonite, Pd^{2+} ions—the required amount of which had been calculated from the adsorption isotherm—were bound to the surface by ion exchange. The amount of ethanol to be used as reductant was determined on the basis of the adsorption excess isotherm of the ethanol–water mixture and the known adequate composition of the nanophase reactor [29–31]. The temperature of montmorillonite dispersions was raised to 65°C before addition of the precursor ions. Palladium particle size was controlled via the metal content. Theoretical and experimentally determined (ICP) Pd contents, the structural parameters of the composites, and particle sizes are listed in Table 1.

Particle size can also be controlled through macromolecules previously adsorbed on the support. Montmoril-

Table 1 Structural parameters of Pd–montmorillonite samples

Sample code	Reductant	Pd content (wt%)	PVP content (wt%)	d_{XRD} (nm)	d_{TEM} (nm)	d_L (nm)
Na–montmorillonite	–	–	–	–	–	1.44
PVPM	–	–	12.4	–	–	1.58
PdM1	Ethanol	0.5 (0.502)[a]	–	10.7	2.2	4.15; 1.49
PdM2	Ethanol	1.0 (0.998)[a]	–	18	4.7	3.74; 1.49
PdM3	Ethanol	2.5 (2.533)[a]	–	22	6.3	3.71; 1.48
PdM4	$NaBH_4$	1	–	–	4.1	3.95; 1.57
PdM5	$NaBH_4$	2	–	–	5.8	1.54
PVPPdM1	Ethanol	2.0 (1.95)[a]	2.1	20.2	5.9	5.68; 1.45
PVPPdM2	Ethanol	2.0 (1.93)[a]	4.1	16.2	3.8	3.24; 1.46
PVPPdM3	Ethanol	2.0 (1.68)[a]	12.4	11.5	2.3	1.54
PVPPdM4	$NaBH_4$	1	3.8	–	2.8	3.82; 1.52

[a] Pd content determined by ICP
d_L Basal distance

lonite is stirred in polymer solution of the adequate concentration for 24 h at 60°C; a mixture of ethanol in mildly acidic aqueous solution of Pd ions [pH=4.0, amount of precursor corresponding to 2% (*m*/*m*) Pd per unit mass of support] is next added. Reduction was also performed, with $NaBH_4$ replacing ethanol as reducing agent.

Compositions of the metal/polymer/montmorillonite composites are presented in Table 1. The metal content decreases with increasing polymer concentration; stabilized metal particles of brownish black color were visually retained in the supernatant after centrifugation.

X-ray diffractograms provide information on polymer adsorption and on the incorporation of nanoparticles formed in the course of reduction. The (001) Bragg reflection is shifted due to interlamellar incorporation of polymers. Basal spacing values of d_L=1.45–1.57 nm were obtained in dried samples containing interlayer alkali or Pd^{2+} ions. The new reflection appearing at larger angles ($d_L = 2.84 - 5.68$ nm) seems to confirm the interlamellar presence of particles as large as 4.7 nm, a value comparable to TEM results. Size distribution functions constructed from the data of TEM images of the samples suggest that the composites may harbor particles measuring even 5–10 nm in diameter. These particles probably grew on the external surfaces (Fig. 1). It is also theoretically possible that we are seeing anisometric expanded ellipsoid or disc-

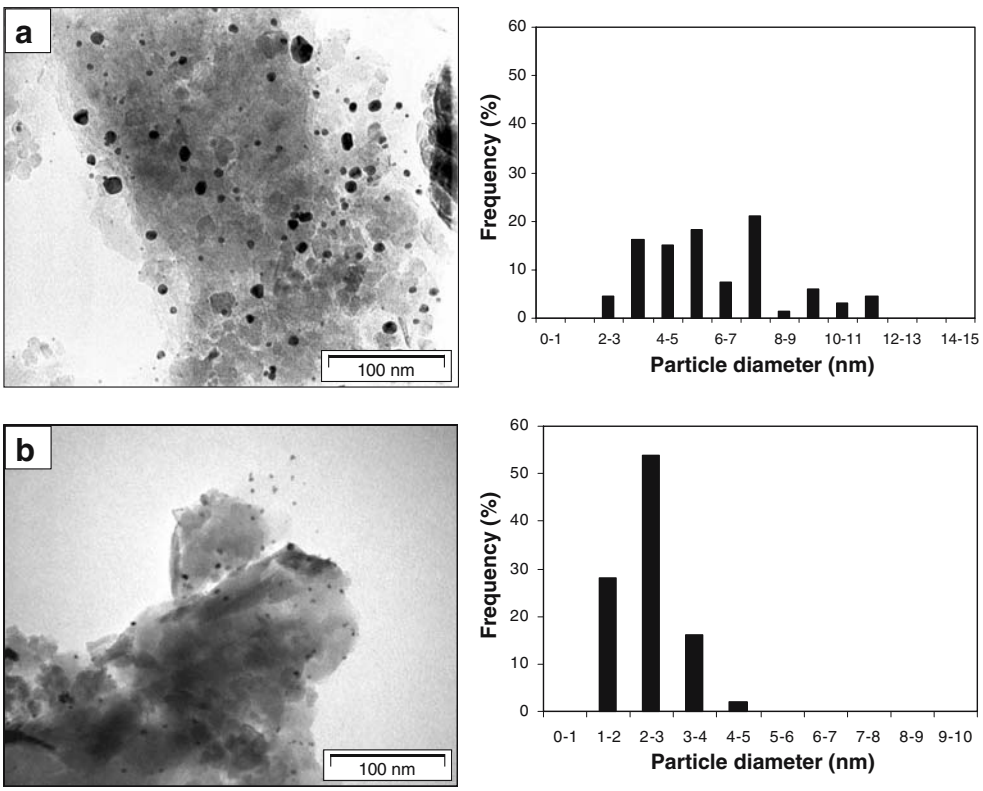

Fig. 1 TEM micrograph and size distribution of Pd–montmorillonites. **a** PVPPdM1 (d_{ave}= 5.9 nm), **b** PVPPdM4 (d_{ave}= 2.8 nm)

shaped particles in the TEM images, whose longitudinal axes (lengths, diameters) may be longer than the values measured by XRD in side view.

Average particle sizes determined by TEM with different metal content are given in Table 1. The addition of stabilizing polymer led to the formation of smaller particles; increasing the amount of polymer further decreased the size. Reduction by $NaBH_4$ led to the formation of smaller particles than did reduction by ethanol (d_{ave}=4.1 and 5.8 nm, respectively). Polymer addition further decreased the particle size also in the case of reduction by $NaBH_4$ (d_{ave}=2.8 and 4.1 nm with and without PVP, respectively).

Thus the size of palladium particles synthesizable on montmorillonite can be successfully decreased by adding polymer to the support in the course of synthesis, before reduction of the palladium ions.

In the X-ray diagram, the (111) reflection characteristic of palladium appears at 40.15° (CuK→). With decreasing particle size, the lattice constant increases, and as a consequence, the position of (111) reflection shifts to smaller two theta values. Particle sizes calculated from the line broadening by the Scherrer equation (10–22 nm) exceed those determined by electron microscopy. The reason is that XRD analyzes the entire sample that may contain large crystallites but fails to observe smaller, amorphous particles.

The role of macromolecules in surface fixation of nanoparticles

As shown in Figs. 2 and 3, molecular coils of PVP are easily adsorbed on montmorillonite lamellae. In polymer solutions with 0.02 mM Pd of 1.5–2.0 nm average diameter, Pd particles with PVP were adsorbed possibly due to reduced expansion of the polymer chains stabilizing the particles.

Adsorption of palladium particles at various polymer/particle ratios was studied in a polymer solution of constant

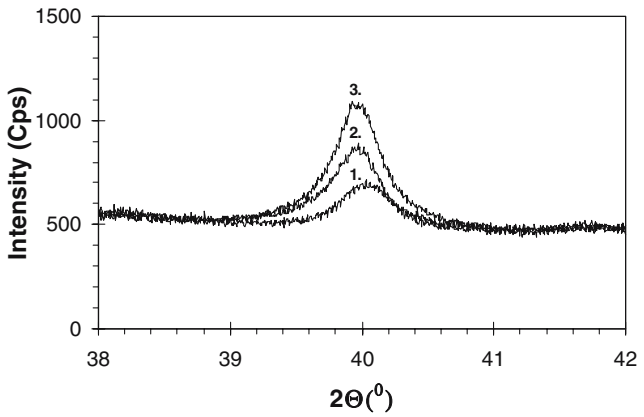

Fig. 2 Pd(111) reflection of the different PVP/Pd/montmorillonite samples (*1*) PVPPdM1, (*2*) PVPPdM2, (*3*) PVPPdM3

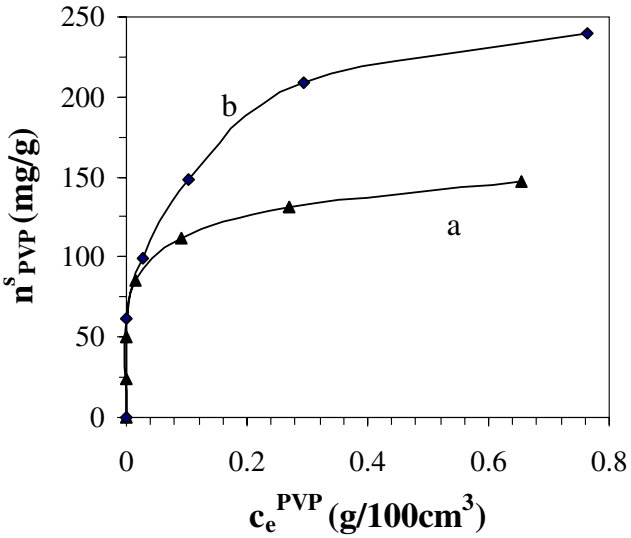

Fig. 3 Adsorption isotherms of (*a*) PVP (*b*) PVP-protected Pd° nanoparticles in aqueous solution on Na–montmorillonite

concentration. At lower polymer concentration, palladium particles were fully adsorbed, and at higher concentration, we have only polymer coils in the equilibrium solution. Incorporation of particles into the interlamellar space was monitored by XRD. Figure 4 shows that the intensity of the basal distance of montmorillonite reflection appearing at 1.42 nm is reduced; the reflection is gradually flattened, whereas the intensity of the new peak appearing at 3.91 nm increases, indicating intercalation of the polymer-coated Pd° particles. The ratios of the intensities of the two peaks ($I_{d=1,42\ nm}$:$I_{d=3,91\ nm}$) at Pd contents of 0.5, 1, 2, and 4% (*m*/*m*) are 2.3, 1.3, 0.8, and 0.3, respectively, a data series that can be considered as a measure of the structural transformation taking place. There is good agreement between the particle diameter calculated from the basal spacing ($d = 3.91\ nm - 0.96\ nm = 2.95\ nm$) and that determined by TEM (2.61 nm).

At the higher polymer concentration (c=0.06 g/100 cm^3), relatively fewer palladium particles can bind to the surface of the support, and more remain, stabilized, in the liquid phase. As shown in Fig. 5, the initial region of the isotherm—i.e. at low Pd° particle concentration (0.12 mmol Pd/dm^3)—particle adsorption will be determined by polymer adsorption. When particle concentration is increased at constant polymer concentration, the attraction due to surface–particle interaction will become dominant, and consequently, more palladium will be adsorbed.

Synthesis of palladium and silver nanoparticles on the surface of disaggregated kaolinite lamellae

The adsorption nanoreactor preparation technique is successfully applicable not only on montmorillonite but also

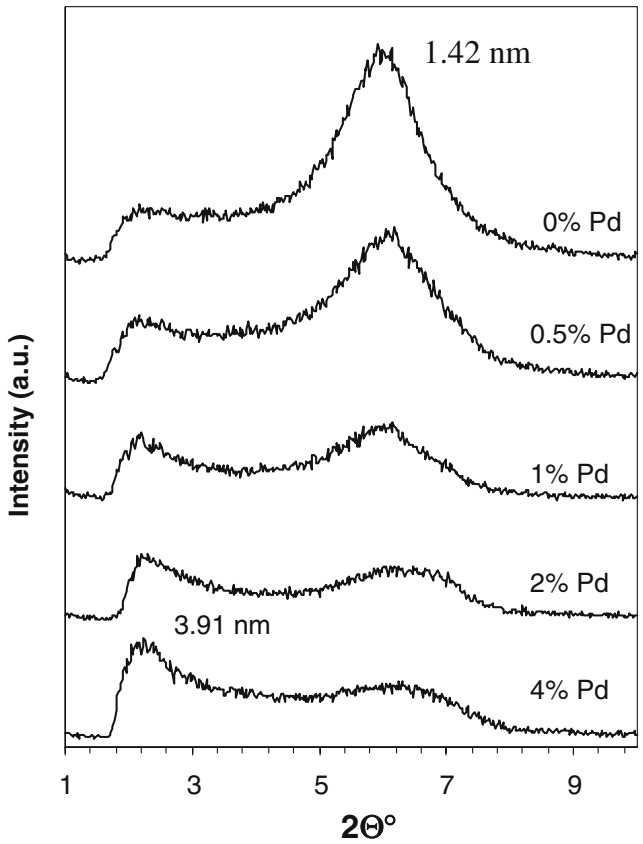

Fig. 4 XRD patterns of polymer-protected Pd–montmorillonite showing Pd particles intercalated in the interlamellar space, at different Pd contents

on kaolinite. A large specific surface area is essential for particle growth and can be created by delamination of kaolinite lamellae. The delamination means the splitting of the particles (lamellae) into the single silicate layers, which is very difficult for kaolinite and only processes in special cases by interaction of very polar solvent. As the lamellar packages of kaolinite are split to elementary lamellae by intercalation of DMSO, the interlamellar space is rendered suitable for the growth of metal nanoparticles. Kaolinite was swollen in DMSO for 24 h at 65°C and alternately washed in fresh methanol and decanted for 5 days. By the evidence of XRD, the (001) basal spacing of kaolinite increased from 0.72 to 1.12 nm (Fig. 6). The interlamellar distance was not altered after washing in methanol, indicating that the intercalated molecules were not removed from between the kaolinite lamellae by washing. The intercalated kaolinite was further used similarly to montmorillonite. The adsorbed Pd^{2+} ions were reduced by hydrazine or Na–borohydride. Reductants were applied in a fourfold excess. The metal contents of the products were 0.95 and 1.9% (*m*/*m*). The silver ions were reduced by $NaBH_4$ and UV irradiation. The amounts of silver added to kaolinite samples were 0.5, 1, 1.5, 2, and 5 g Ag/100 g kaolinite. The compositions and structural parameters of the samples are shown in Table 2.

The presence of Ag nanoparticles in the supernatants was tested by UV-VIS spectroscopy. It may be assumed that in the lower Ag concentrations (0.5–2%) all nanoparticles were formed on the surface of the support, whereas at higher Ag concentrations (5%) not all Ag^{+} ions can be adsorbed on the kaolinite lamellae; therefore silver nanoparticles are also generated in the liquid phase. When hydrochloric acid was dripped into the supernatant after centrifugation, no AgCl precipitate was formed, which

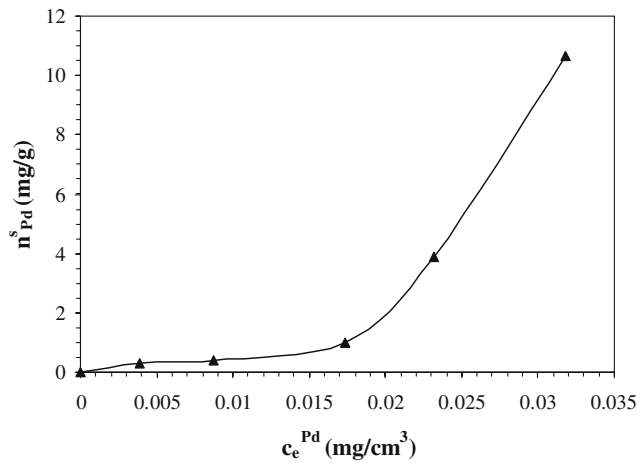

Fig. 5 Adsorption isotherm of Pd nanoparticles stabilized by PVP in aqueous solution on Na–montmorillonite at 0.06 g/100 cm^3 PVP concentration

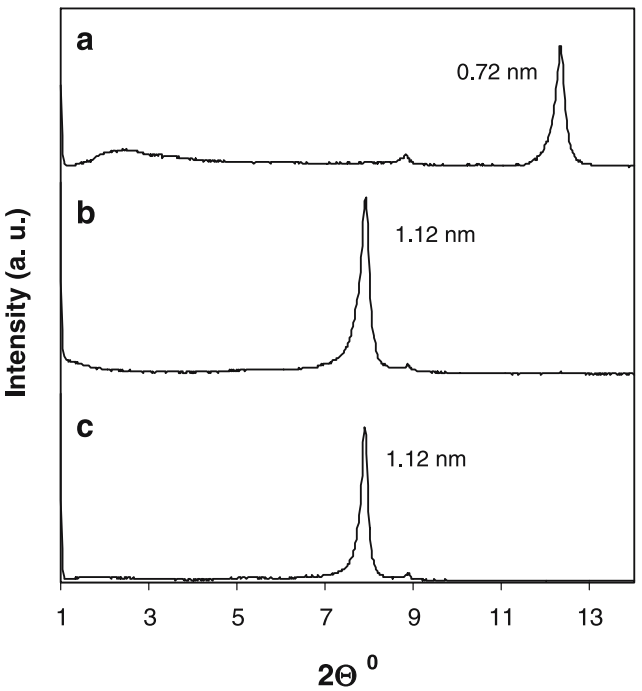

Fig. 6 XRD patterns of kaolinite (*a*), DMSO-treated kaolinite (*b*), and DMSO-treated kaolinite after washing by methanol (*c*)

Table 2 Structural parameters of Pd–kaolinite samples

Sample code	Reductant	Pd content (wt%)	PVP content (wt%)	d_{TEM} (nm)	d_L (nm)
Kaolinite	–	–	–	–	0.72
DMSOK	–	–	–	–	1.12
PVPK	–	–	1.9	–	3.64; 0.72
PdK1	Hydrazine	0.95	–	7.2	4.13; 0.73
PdK2	Hydrazine	1.90	–	14.3	5.33; 0.72
PVPPdK1	Hydrazine	0.95	3.8	2.8	0.72
PVPPdK2	Hydrazine	1.90	3.8	5.8	4.36; 0.72
PVPPdK3	Hydrazine	0.95	28.0	2.6	4.21; 0.72
PVPPdK4	$NaBH_4$	0.95	3.8	4.7	4.62; 0.72
PdK3	$NaBH_4$	0.95	–	6.0	5.95; 0.73
PdK4	$NaBH_4$	1.90	–	8.1	6.87; 0.73

d_L Basal distance

means that reduction had proceeded to completion, as no Ag^+ ions remained in the dispersion.

Disaggregation and the structural change due to nanoparticle incorporation between kaolinite lamellae can be conveniently monitored by XRD (Figs. 6 and 7). After the adsorption of PVP, the reflection characteristic of DMSO-treated kaolinite disappeared because the DMSO desorbed from the interlamellar space. The original (001) kaolinite reflection appeared, although at a reduced intensity. The intensities of reflections are markedly lower, and their half-widths are larger in samples containing PVP and/or nanoparticles than in the original clay mineral containing no silver particle formation disrupting some of kaolinite layers. The X-ray diffractograms reveal an interesting mechanism

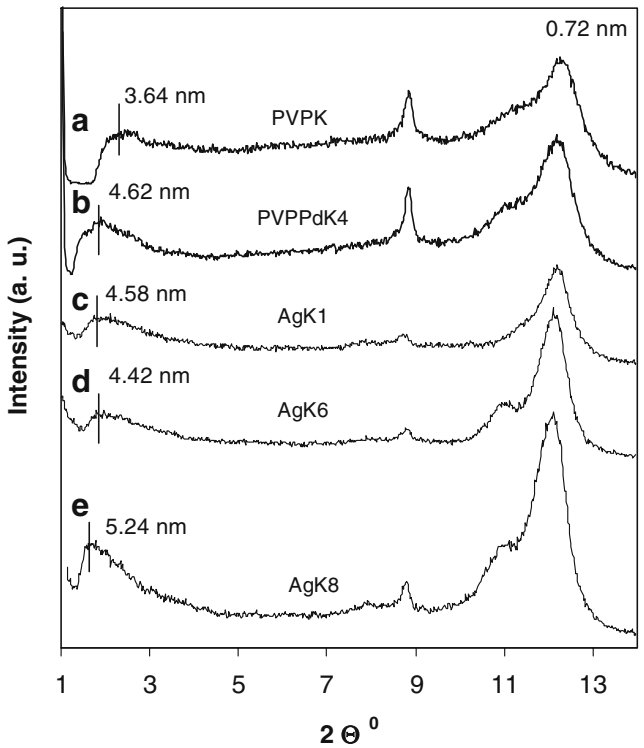

Fig. 7 XRD patterns of PVP, Pd, and Ag intercalated kaolinite samples

of particle formation in layered compounds. The presence of two reflections, even broadened of reduced intensity, indicate that particle formation does not occur randomly in some interlayer spaces but in a certain number of neighboring interlayer spaces so that more or less ordered packets with interlayer metal particles alternate with less ordered packets of unreacted kaolinite layers. In other words, there is a certain segregation of the nanoparticles separated by kaolinite layers. On X-ray diffractograms of palladium-containing composites, the interlamellar localization of metal clusters is evidenced by a shift of the reflection (d_L=3.6 → 4.6 nm; Fig. 7). The basal spacing can reach values as high as 6.84 nm (Table 2).

Comparison of the X-ray diffractograms of samples with identical silver contents prepared by two methods of reduction reveals significant differences. After photochemical reduction, the intercalation reflection is sharper and more intensive at each Ag concentration. The reason for this is that a larger proportion of Ag particles were formed in the interlamellar space, and these particles are larger than d_L=5.64 nm (Table 3).

Although the dimensions of the interlamellar space limit particle growth, we still observed in TEM pictures particles exceeding this limitation: these particles must have formed on the external surface of the clay mineral. Pseudohexagonal plate crystals characteristic of kaolinite are well discernible in TEM images (Fig. 8). PVP addition decreased the particle size. TEM images of samples PVPPdK1 and PVPPdK4 display spherical particles measuring 2–6 nm, situated separately on the lamellae, with no sign of aggregation (Fig. 8a). When metal content is increased (Fig. 8b), strings of metal particles are seen to cling to the edges of the kaolinite lamellae, whereas the particle diameter is not modified significantly. This allows to conclude that the part of polymer chains, which could not be adsorbed on kaolinite, remained in the bulk phase and stabilized the particles formed in the course of reduction. These "large" units could only attach to the external surface of the lamellae. When palladium content is

Table 3 Structural parameters of Ag/kaolinite samples

Sample code	Reductant	Ag content (wt%)	d_L (nm)	d_{XRD} (nm)	d_{TEM} (nm)
AgK1	$NaBH_4$	0.5	4.58	10.7	5.6
AgK2	$NaBH_4$	1.0	4.28	12.7	7.1
AgK3	$NaBH_4$	1.5	4.24	13	7.6
AgK4	$NaBH_4$	2.0	4.39	13.1	8.3
AgK5	$NaBH_4$	5.0	4.95	24	10.5
AgK6	Photoreduction	1.0	4.42	10.1	8.3
AgK7	Photoreduction	2.0	5.64	10.2	8.7
AgK8	Photoreduction	5.0	5.24	11.3	11.2
AgK9	Photoreduction	10.0	3.69	10.1	14.8

d_L Basal distance

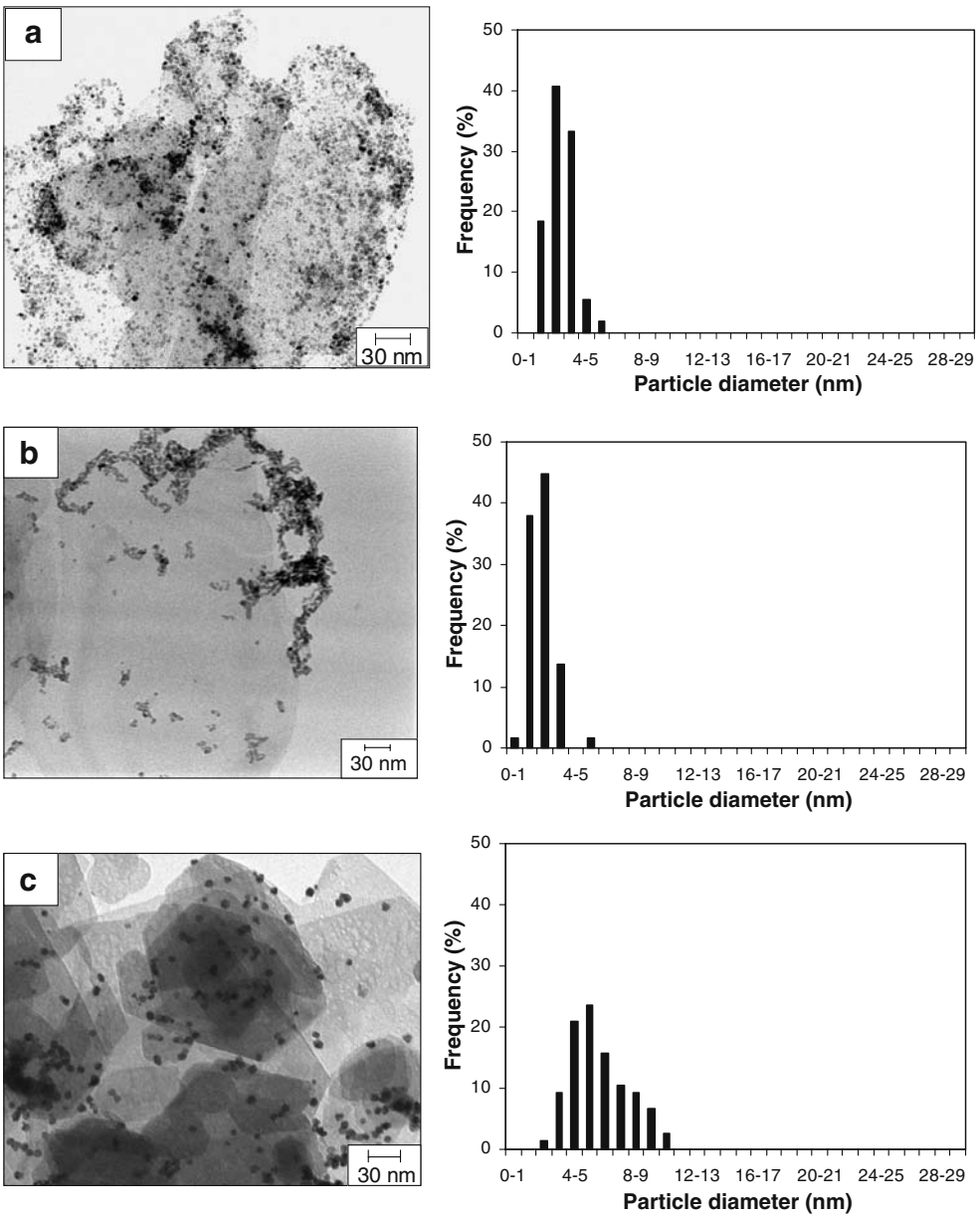

Fig. 8 TEM micrograph and particle size distribution of **a** PVPPdK1 (d_{ave}=2.8 nm), **b** PVPPdK3 (d_{ave}=2.6 nm), **c** PdK1 (d_{ave}=7.2 nm), **d** PdK2 (d_{ave}=14.3 nm), **e** AgK4 (d=8.3 nm), **f** AgK6 (d=8.7 nm)

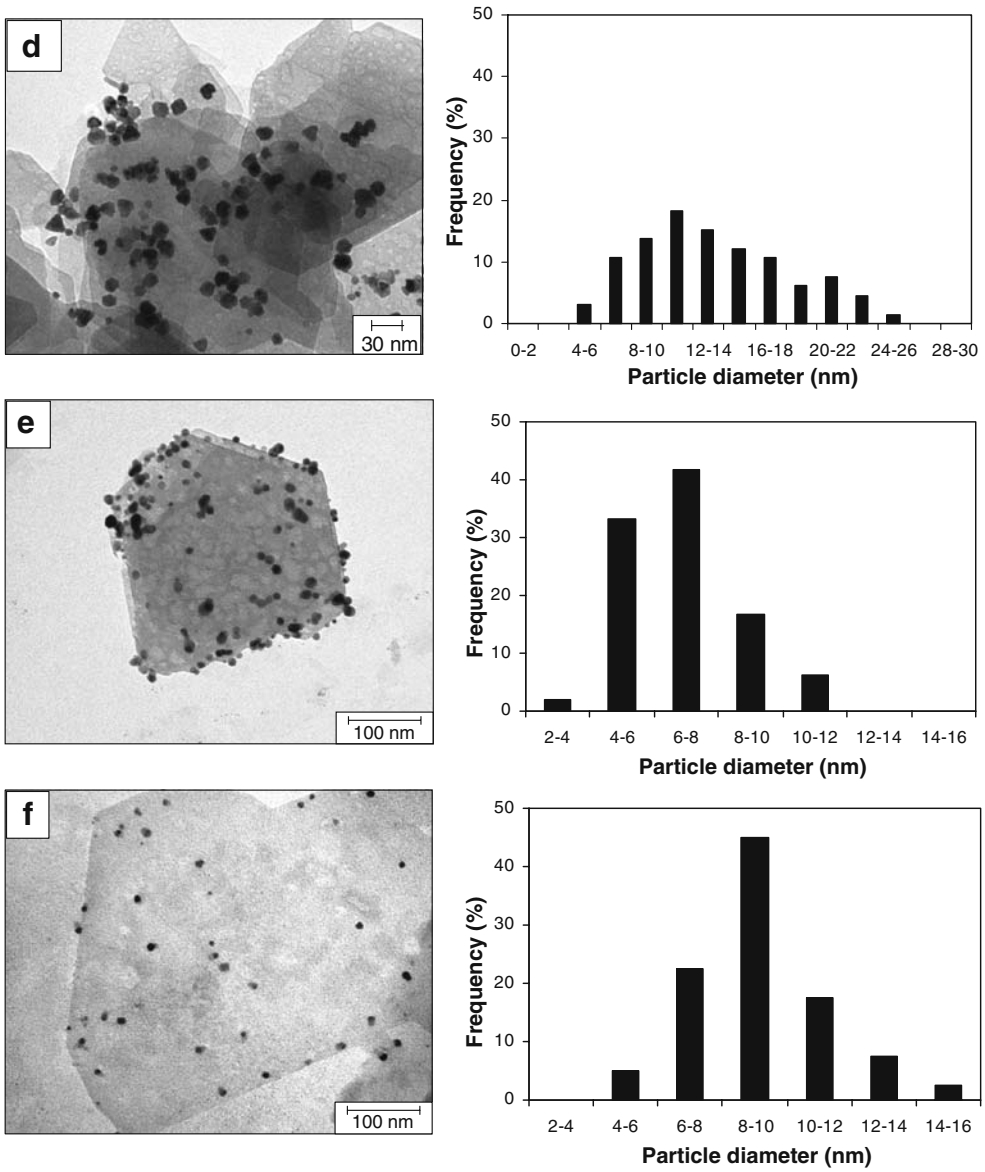

Fig. 8 (continued)

increased at constant polymer content, larger particles are formed (0.95% → 2.8 nm; 1.9% → 5.8 nm, see Table 2). When palladium content is raised to 2% without polymer stabilization and the slower reduction method (hydrazine) is applied, crystalline particles of diversified morphology measuring as large as 20–30 nm are formed.

The average size of silver nanoparticles also increases with increasing metal content: d_{TEM} was 5.6 nm in sample 0.5 AgK and 10.5 nm in sample 5 AgK. In accordance with the results of XRD, photoreduction resulted in the formation of larger particles than reduction by sodium borohydride. TEM images reveal (Figs. 8e,f) that particles are scattered more sparsely on photoreduced samples because slower reduction favored particle growth. In contrast, sodium borohydride added in excess rapidly reduced all Ag^+ ions present; particle growth was therefore favored over nucleation, leading to the formation of a larger number of smaller particles.

The (111) Ag Bragg reflections (2Θ=38.3°) revealed that peak intensities increase and half-widths decrease with increasing the silver content of the samples because the size and crystallinity of silver particles increase (see Fig. 9). Average particle sizes calculated by the Scherrer equation are somewhat larger ($d_{XRD} = 10.7 - 24\ nm$) than those obtained by evaluation of TEM images ($d_{TEM} = 5.6 - 10.5\ nm$). The reason for this discrepancy is that the average particle diameter determined by X-ray diffractometry is a so-called mass-weighted average that yields a higher numeric value than the number-weighted average particle size derived from TEM images.

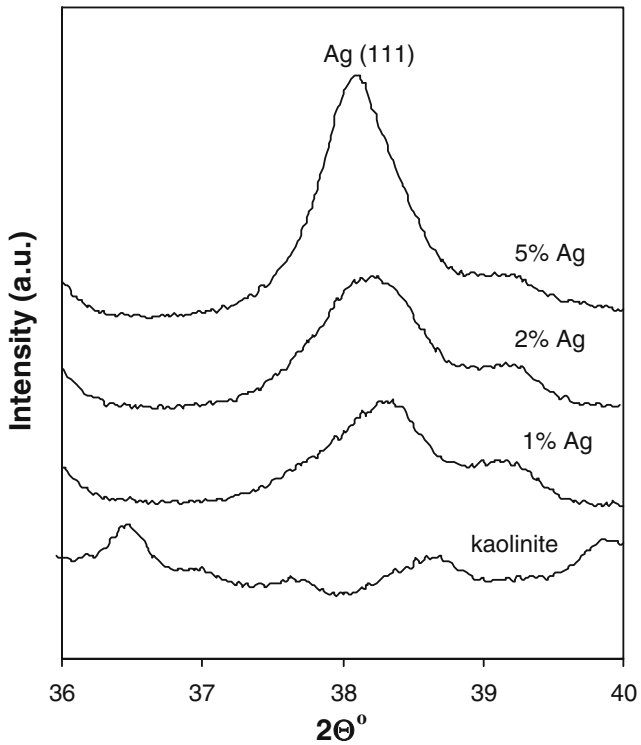

Fig. 9 Ag(111) reflection of the different Ag/kaolinite samples

Analysis of palladium and silver nanoparticles by X-ray photoelectron spectroscopy

XPS studies were aimed at the assessment of the surface oxidation state of the particles. Figure 10 displays the spectra of samples PdM5 and PdK4 resolved to the lines of the Pd° and Pd^{4+} oxidation states. Input parameters are the binding energies of Pd $3d_{3/2}$ peaks, the difference of the binding energies of the Pd $3d_{3/2}$ and Pd $3d_{5/2}$ peaks, and the ratio of the intensities of the two peaks. Half-widths were identical for each peak in the different samples.

In addition to the peaks at 335.0 and 340.6 eV corresponding to the binding energies attributable to the doublets of $3d_{3/2}$ and Pd $3d_{5/2}$ of palladium in zero oxidation state, peaks also appear at 337.7 and 342.7 eV. These peaks are characteristic of the Pd^{4+} oxidation state. In addition to metal atoms in zero oxidation state, all Pd-containing catalysts studied contain ions in the Pd^{4+} oxidation state. This indicates that PdO is not formed on the surface, but Pd° and PdO_2 are present. Thus either only part of the metal ions added were reduced in the course of synthesis, or all metal ions were reduced, but some of them converted to metal oxide by reacting with oxygen on the surface. It cannot be excluded that the presence of forms in higher oxidation states is due to a metal–support interaction on the surface.

Ag 3d X-ray photoelectron spectra (XPS) of the samples with different silver contents are presented in Fig. 11. Binding energies of Ag $3d_{5/2}$ peaks were in the range of 367.7–367.9 eV, whereas those of Ag $3d_{3/2}$ peaks were in the range of 373.75–373.9 eV. The position of the peak is characteristic of metallic silver and is independent of silver concentration. Full widths at half maximum (FWHM) ranged from 1.81–1.83 eV, except for sample 5 AgK that displayed a value of 1.68 eV. Binding energies and values of FWHM were within the limits of experimental error.

As peak areas are directly proportional with the number of atoms present, the areas allow estimation of the silver content of the samples. The magnitude of the Ag 3d peak as a function of theoretical silver content is shown in Fig. 12. It is clearly seen in the figure that the function is linear up to 2% Ag^+ content and then bends towards the *x*-axis, indicating that the actual silver content is lower than the value expected on the basis of the amount of Ag^+ added. This is in accordance with the spectrophotometric results; i.e., above a certain concentration no more Ag^+ ions can be

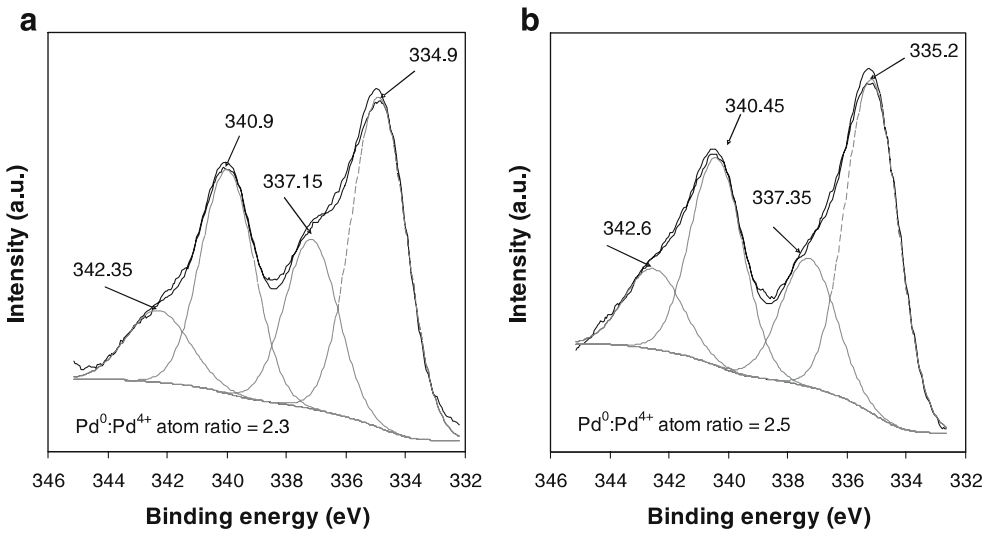

Fig. 10 XPS Pd3d spectra of Pd°–montmorillonite PdM5 (**a**) and Pd°–kaolinite samples PdK4 (**b**)

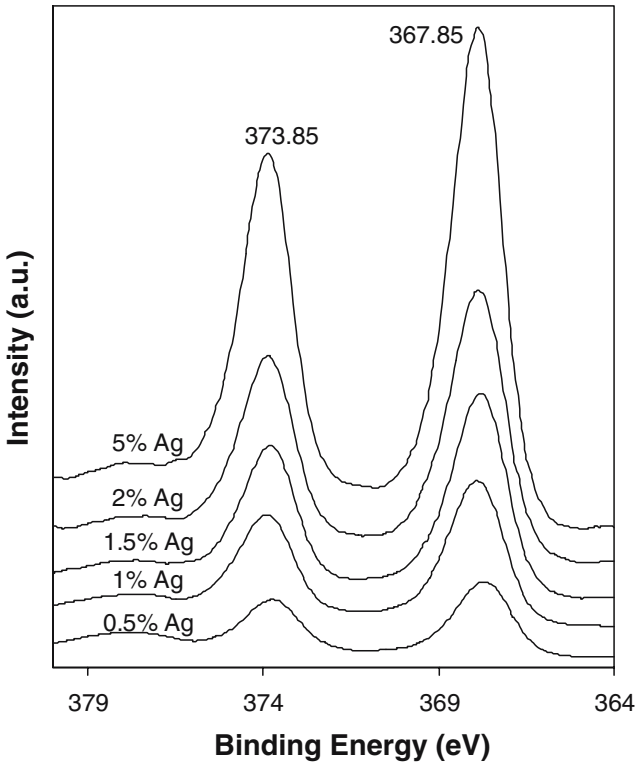

Fig. 11 Ag 3d X-ray photoelectron spectra of Ag/kaolinite samples (0.5, 1, 1.5, 2, and 5% Ag contents)

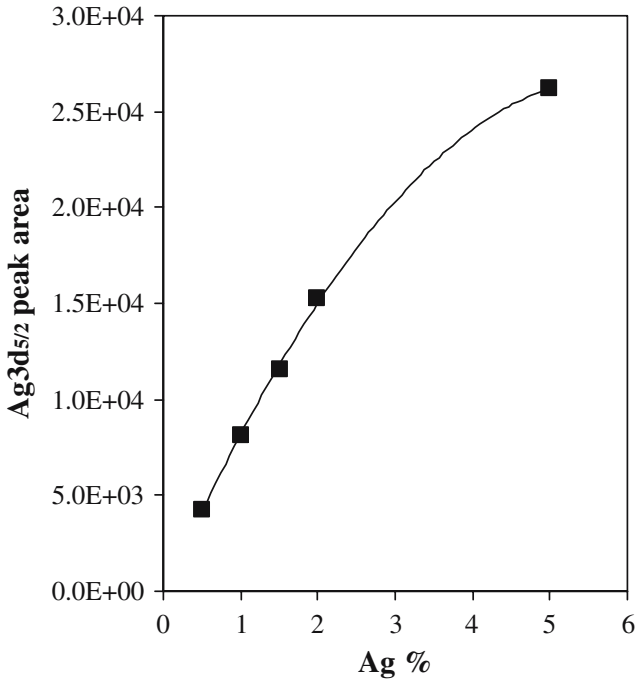

Fig. 12 Ag 3d peak area of Ag/kaolinite samples as a function of Ag content

adsorbed on the surface of kaolinite; therefore particles are also formed in the liquid phase.

Conclusion

Palladium and silver nanoparticles were synthesized on the surface of Na–montmorillonite and kaolinite lamellae. Metal nanoparticles can be conveniently incorporated into lamellar kaolinite if the interlamellar spaces were previously expanded by dimethyl sulfoxide. Palladium chloride was reduced by ethanol, hydrazinem, or sodium borohydride. XRD measurements revealed the appearance of a new Bragg reflection in the small angle range in the course of the heterogeneous nucleation of nanoparticles, confirming that nanoparticles were also formed in the interlamellar space. The presence of this reflection, even broadened and of weaker intensity, indicates a certain segregation of the nanoparticles in packets of kaolinite layers. The size of particles formed by heterogeneous nucleation increased with increasing metal content. Reduction by sodium borohydride resulted in the formation of smaller particles than did reduction by ethanol or hydrazine. Photoreduction of silver also led to the formation of large particles. Photoreduction is a relatively slow process, creating favorable conditions for particle growth. When polymer had been added before reduction, the particle size could be decreased by increasing polymer concentration. In this case, the stabilizing effects of both the support and polymer cooperate.

At low polymer concentrations, the particles of polymer-protected palladium particles not only attached to the external surface of the lamellae but also were incorporated between the lamellae of the clay mineral. The number of incorporated particles decreased with increasing polymer concentration. At high polymer/particle ratios, polymer adsorption suppressed nanoparticle binding. At low polymer/particle ratios, attraction due to the particle–surface interaction dominated, causing more Pd° particles to be adsorbed on the surface.

The surface oxidation state of the metal particles was determined by XPS. Silver was shown to be present in the samples in zero oxidation state, whereas the surface of palladium particles was partially oxidized in all cases. In addition to metallic palladium, PdO_2 was also present. These results indicate that either only part of the Pd^{2+} ions applied to the support were reduced in the course of synthesis, or all ions were reduced but some ions converted to metal oxide by reacting with oxygen on the surface. It cannot be excluded that the presence of forms in higher oxidation states is due to a metal–support interaction on the surface.

Acknowledgement The authors wish their thanks for the financial support of the Péter Pázmány Program of the Hungarian National Office of Research and Technology (number RET-07/2005).

References

1. Bradley JS (1994) Clusters and colloids: From theory to application In: Schmid G (ed) VCH, New York, pp 459–536
2. Rampino LD, Nord FF (1941) J Am Chem Soc 63:2745
3. Boutonnet M, Kizling J, Stenius P, Maire (1982) Colloids Surf 5:209
4. Wang CC, Chen DH, Huang TC (2001) Colloids Surf A 189:145
5. Nickel U, Castell A, Pöppl K, Schneider S (2000) Langmuir 16:9087
6. Zhao MQ, Crooks RM (1999) Chem Mater 11:3379
7. Naka Y, Kaeriyama K (1986) J Colloid Interface Sci 110:86126
8. Pillai ZS, Kamat PV (2004) J Phys Chem B 108:945
9. Heard SM, Grieser F, Barraclough CG, Sanders JV (1983) J Colloid Interface Sci 93:545
10. Hoogsteen W, Fokkink LGJ (1995) J Colloid Interface Sci 175:12
11. Hirai H, Nakao Y, Toshima N (1979) J Macromol Sci Chem A13:727
12. Teranishi T, Miyake M (1998) Chem Mater 10:594
13. Wilcoxon JP, Williamson RL, Baughman R (1993) J Chem Phys 98:9933
14. Parsapour F, Kelley DF, Craft S, Wilcoxon JP (1996) Phys Chem 104:4978
15. Pocard NL, Alsmeyer DC, McCreery RL, Neenan TX, Callstrom MR (1992) J Am Chem Soc 114:769
16. Steigerwald ML, Brus LE (1990) Acc Chem Res 23:183
17. Cheomg Chan YN, Schrock RR, Cohen RE (1992) Chem Mater 4:205
18. Zhao M, Sun L, Crooks RM (1998) J Am Chem Soc 120:4877
19. Bönnemann H, Braun G, Brijoux W, Brinkmann R, Schulze TA, Seevogel K, Siepen KJ (1996) Organomet Chem 520:143
20. Reetz MT, Helbig WJ (1994) J Am Chem Soc 116:7401
21. Reetz MT, Quaiser SA, Breinbauer R, Tesche B (1995) Angew Chem Int Ed Engl 34:2240
22. Wang Q, Liu H, Wang H (1997) J Colloid Interface Sci 190:380
23. Wang Y, Liu H, Huang Y, (1996) Polym Adv Technol 7:634
24. Dékány I, Turi L, Szűcs A, Király Z (1998) Colloids Surf A 141:405
25. Papp Sz, Szűcs A, Dékány I (2001) Appl Clay Sci 19:155
26. Király Z, Dékány I, Mastalir Á, Bartók M (1996) J Catal 161:401
27. Szűcs A, Király Z, Berger F, Dékány I (1998) Colloids Surf A 139:109
28. Király Z, Veisz B, Mastalir Á, Rázga Zs, Dékány I (1999) Chem Comm 1925
29. Papp Sz, Szűcs A, Dékány I (2001) Appl Clay Sci 19:155
30. Dékány I, Farkas A, Király Z, Klumpp E, Narres HD (1996) Colloids Surf A 119:7
31. Dékány I, Ábrahám I, Nagy LG, László K (1987) Colloids Surf A 23:57